

Study of high energy phenomena from near space using low-cost meteorological balloons

Sandip K. Chakrabarti · Ritabrata Sarkar ·
Debashis Bhowmick · Arnab Bhattacharya

Abstract Indian Centre for Space Physics has taken a novel strategy to study low energy cosmic rays and astrophysical X-ray sources which involve very light weight payloads up to about five kilograms on board a single or multiple balloons which are usually used for meteorological purposes. The mission duration could be anywhere from 3-12 hours. Our strategy provides extreme flexibility in mission preparation and its operation using a very economical budget. There are several limitations but our innovative approach has been able to extract significant amount of scientific data out of these missions. So far, over one hundred missions have been completed by us to near space and a wealth of data has been collected. The payloads are recovered and are used again. Scientific data is stored on board computer and the atmospheric data or payload location is sent to ground in real time. Since each mission is different, we present here the general strategy for a typical payload and provide some results we obtained in some of these missions.

Keywords X-ray detectors and instrumentation · Secondary cosmic ray · X-ray sources · Meteorological balloon borne mission

PACS 94.20.wq · 94.05.Sd · 95.55.-n · 95.55.Ka · 96.60.Q

1 Introduction

Study of the Universe in X-rays is a very important regime of astronomical observations. Since the atmosphere surrounding the earth obscures X-ray, we need to reach

Sandip K. Chakrabarti · Ritabrata Sarkar · Debashis Bhowmick · Arnab Bhattacharya
Indian Centre for Space Physics, 43 Chalanika, Garia Station Rd., Kolkata 700084
Tel.: +91-33-24366003
Fax: +91-33-24622153 Ext. 28
E-mail: ritabrata.s@gmail.com

Sandip K. Chakrabarti
S.N. Bose National Centre for Basic Sciences, JD Block, Salt Lake, Kolkata 700097
Tel.: +91-33-23355706
Fax: +91-33-23353477
E-mail: sandipchakrabarti9@gmail.com

above it. For more than hundred years, balloons are being used for this purpose to study Cosmic Ray (CR) and high energy phenomena of the Universe. More expensive satellite missions with on board payloads provide astronomers a platform to carry out experiments which can do longer observations. These missions are expensive and require a very long preparation time.

With the advent of miniaturization of instruments, and at the same time improvement of technology to produce low cost balloons, it has become now possible to investigate the high energy universe using very light-weight payloads. Successful recovery of payloads make the instruments reusable rendering the cost even lower and within the reach of colleges and university budgets. While our integrated payloads are less than about 5 kg, some of the science-return has been rewarding. Because of light-weight, pointing had to be sacrificed, but our innovative approach allows us to separate photons from each object of interest. Certainly, some scientific goals which require longer observations, larger areas or precession pointing are sacrificed, but repeatability at a low cost enables us to study very long time scale variability (such as cosmic ray variation with solar activity for several years) which are not possible by a single satellite mission (*Sarkar et al.*, 2017). In addition, our method allows us to evaluate, test and improve each payload in a near space environment before being used in space. Several preliminary reports of our activities are given in *Chakrabarti et al.* (2011, 2013, 2014, 2015).

In this paper, we describe the overall mission strategy, configuration of a typical payload and give examples of typical results obtained by such a payload. In the next Section (§2), we present the overview of such missions. The detailed description of the payload components and their properties are discussed in §3. Then in §4 we discuss the test and calibration of the payloads. In §5.1 we show and discuss typical results, namely, spectrum, light curve and other byproducts from such missions. Finally, in §6, we make concluding remarks.

2 Mission description

2.1 General philosophy

Our motivation is to carry payloads which are no more than about 5 kilograms and to use light weight (1 to 2 kg category) rubber or plastic balloons of about 4000 cubic meters category which are generally used for meteorological purposes. Our science goal is to concentrate on the X-ray sky, though similar fruitful science could be done in any wave band. Our requirements are therefore very stringent in the sense that further in the sky we send our payloads, lesser is the absorption due to the atmosphere and lower is the detectable energy band in X-rays. To this effect, we typically fly from 35 to 42 km.

Each payload, apart from the X-ray instrument in question, must have the data acquisition system, an attitude measure measurement system, GPS system transmitting the instantaneous locations to the ground, parachutes (for rubber balloons), one or more optional video cameras, an optional sun-sensor etc. If the payload is heavier than 2.5 kg, we use two balloons with suitable (to be discussed below) lifts. To

have higher buoyancy, we use hydrogen gas for filling the balloons. So far, we flew our Dignity series of payloads which are used for Cosmic rays and X-ray Universe, 101 times and except for a couple of missions in early days when our expertise were limited, all the payloads have been successfully recovered.

We designed the balloon borne payload to be compact, light-weight, reusable and most importantly of low-cost. Indeed, typically we are able to fly 10-15 times per year in typically two preferred seasons when easier recovery is possible. Construction of a high-altitude balloon-borne payload must take care of the following design constraints. At higher altitudes, the temperature becomes cryogenic. Under that environment, most of the general purpose electronic devices and power supplies are expected to fail and all circuits calibrations on ground are changed. The response of the detectors would also vary. Thus the payload box must be provided with a temperature shielding and the system should be tested to withhold the pressure variation as the mission reaches from ~ 1000 mbar to ~ 2 mbar. Since the mission is expected to be of few hours, and could also be at night time, solar cells are not used.

Styrofoam (thermocool) is a very common widely available heat insulator with a thermal conductivity of only $0.029 \text{ W/m}^\circ\text{C}$ and is of considerably low-cost. Thermocol is a smooth and soft, light weight, material enabling us to curve out areas where specific payloads or circuit boards are to be placed. It has a good amount of strength, and yet, has the ability to absorb some mechanical shock of possible impact with earth during landing. Because of these features, it is the perfect choice for our payloads. All the electronics and detector are also covered with separate thermocol boxes for extra protection. Typically, our payloads remain at $10 - 15^\circ\text{C}$ inside the box throughout the journey.

During our long experience with payload boxes of various shapes and sizes, judging from the data on turbulence experienced in its journey, especially during crossing the tropopause, we found it better to choose the shape of the payload to be cylindrical. The base of the cylinder is flat where electronics components and power supplies rest. On the top surface we place the collimator for the X-ray detector, whenever needed. It may also contain GPS antennas, sun sensor and video camera. Side walls may also have cameras whenever needed. Bottom surface has an extra protection of semi-hard plastic cylinders to absorb shocks during landing.

2.2 Dependence of Balloons and flight-times on Mission goals

One of the major flexibilities of our method is that the launching location need not be fixed. Indeed, we shift the launching location among one of the 4 – 5 chosen places, depending on the wind pattern and the desired landing location. The landing location strongly depends on the wind pattern and changes significantly from day to day, and most certainly, also on whether both balloons burst or a single balloon bursts. Our mission purpose dictates the time of the lift off and that also shifts the landing location within a given day. Mission aim decides the payload weight. Typically, for lighter weight (combined weight of the payload components with parachute less than about 2.5 kg) we fly the missions with a single meteorological balloon. The flight duration is short (up to about 3 hours) as the balloon starts descending right after the

burst. However when the payload is of intermediate weight (e.g., 3 – 3.5 kg), we send two balloons tied up with lifts in such a way that one bursts first and the other brings the payload down slowly, and even float at a near neutrality height for a considerable time. These missions are of longest durations. We experimented with a case of 12 hours of flight with two balloons. However, typical duration is about 5 – 6 hours. The landing location has to be predicted very carefully depending on the lifts given and whether or not near neutrality is achieved. Of course, when GPS is attached, it becomes easier for the recovery team to collect the payload in real time as it lands.

When the payload is heavier, say 4 kg or more, we either send two rubber balloons with appropriate lifts so that both burst simultaneously and the trajectory is close to that predicted for a single balloon. Even when one bursts, the heavy payload is brought down by the other, merely an hour or so late. So the flight duration is about 3 – 4.5 hours in this case. However, if we are interested to have longer duration data at greater height (say above 30km), we prefer to use a single polythene balloon which can stay about 4 – 5 hours in flight with about an hour above 30 km. We use TIFR, Hyderabad made 4000 cubic meter category balloons for this purpose. Since a polythene balloon does not burst as a rubber balloon, and also does not require any parachute, its trajectory is quite different from those flights having rubber balloons. These balloons also require a larger launching ground. More than two smaller polythene balloons have been tried by us also. However, the predictability of such balloons is not high and recovery becomes more complex. So, we do not recommend using more than two balloons without ejection mechanism, unless there are specific requirements for such a configuration. They tend to go to lower height also, mainly due to uneven load on each balloon during air turbulence.

The schematic picture of different types of carrier balloons and their combinations to carry the payload are shown in Fig. 1. In case of the stretchable rubber balloons the payload is suspended by a rope at the end of the balloon with a parachute inserted in between the balloons and the payload.

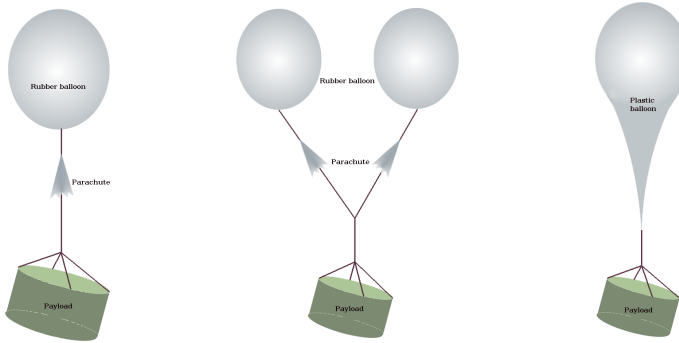


Fig. 1 Different carrier configurations used in the flights. Left: single rubber balloon (~ 10 ft diameter on the ground); middle: double rubber balloon; right: About 100 ft long polythene balloon.

In Fig. 2 we show the real pictures of three kinds of carrier combinations. A

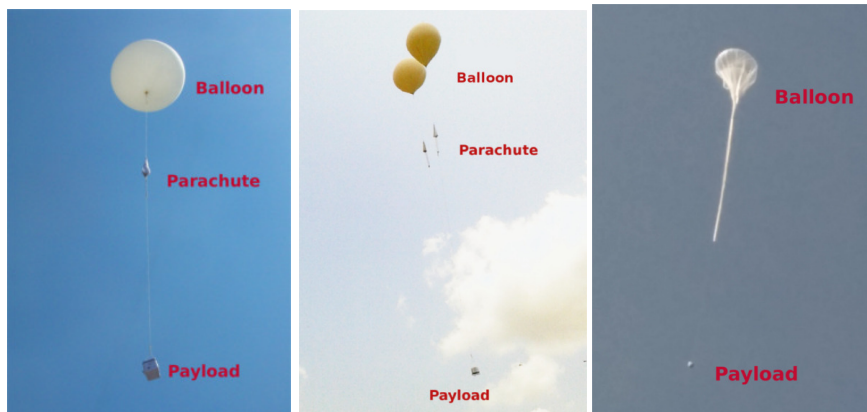


Fig. 2 Balloons and payload photos just after launch. Left: single rubber balloon; middle: double rubber balloon; right: bigger polythene balloon. Individual parachutes are attached to each of the double balloons to avoid possible crash landing.

picture of typical landing with the parachute is shown in Fig. 3.

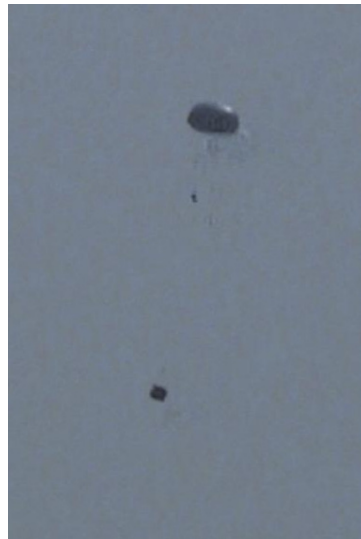


Fig. 3 Example of a Parachute (D17) carrying the payload back to the ground.

2.3 Trajectory

The overall flight path depends on the duration of the flight and the wind condition and we can roughly predict the path using one of the numerous balloon flight path

predictors. They generally predict the landing location for a single balloon, but in complex situations such as ours, we use our own software to predict the location depending on the lifts given at launch.

Single balloon landing prediction routines such as the Cambridge University (*CUSF Landing Predictor*, 2016) tool helps us to choose suitable launching location in order that the landing is at a desired place for safer payload recovery. Typically, in our geographical location of launching, namely, Bolpur, West Bengal (India) having (Latitude: 23.67N, Longitude: 87.68E) and in its vicinity, there are two windows of opportunity for launching per year each of which last for about a month. One is in April-May, in the pre-monsoon season, and the other is in October-November, in the post-monsoon season. Of course, we flew at other times as well (Fig. 4). In Fig. 4 we show a plot of the launching and landing locations for the missions we conducted so far. Only the end points and not the the actual paths are shown.

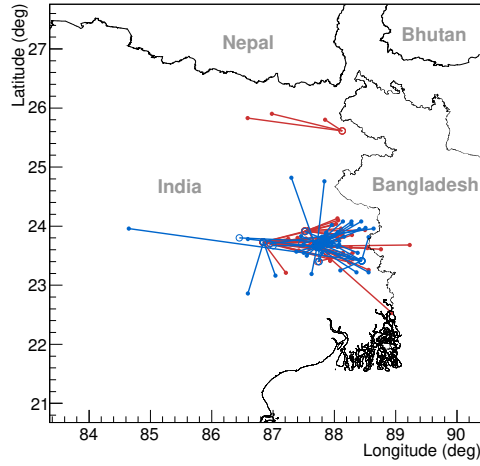


Fig. 4 Distribution of the launching (open circles) and landing locations (filled circles) of the payloads. Missions during the Jul-Feb are shown by red and those during the Mar-Jun are given by blue.

We rely on the transmitted GPS data every 30 seconds to get the actual locations. However, whenever the weight restriction constrains us, we use only the GPS locator service through local cell phone network to get the landing location. These allow us to have almost a hundred percent recovery. Because of international boundaries nearby, we restrict to these two launching slots. In future, we plan to shift launching towards central India to have round the year launching without any problem.

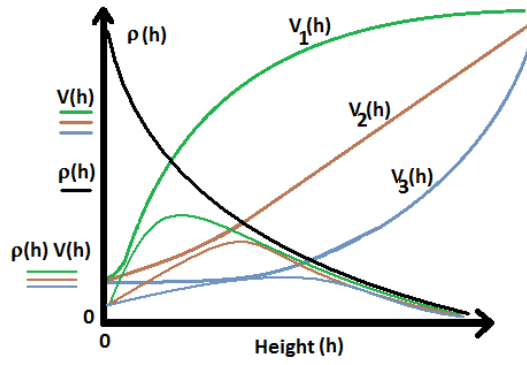


Fig. 5 Schematic behaviour of the air density $\rho(h)$, balloon volume $V(h)$, and the lift $\rho(h)V(h)$ as a function of height for three types of expansion of the balloon with height. All quantities are in arbitrary units.

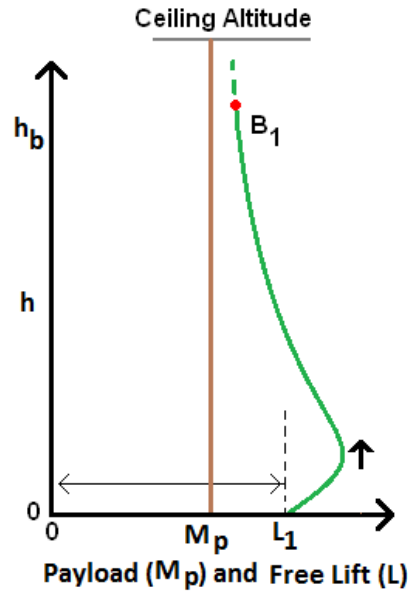


Fig. 6 Schematic behaviour of $\rho(h)V(h)$ of a general balloon with altitude showing that the lift has a maximum at an altitude and then starts decreasing monotonically till the burst height.

2.4 Behaviour of Lifts in a single and a double-balloon configuration

In a single balloon with the configuration shown in Fig. 1 (left), the effective free lift is given by

$$L = \rho(h)V(h) = M_p \frac{a}{g} - M_H,$$

where, $V(h)$ and $\rho(h)$ are the volume of the balloon and the density of air respectively at the instantaneous height h ; M_p and M_H are the masses of the payload ($M_p = M_i + m$; M_i = mass of the instrument box; m = mass of the parachute) and M_H = mass of the hydrogen gas inside the balloon. a is the acceleration in which the payload lifts off and g is the acceleration due to gravity.

In Fig. 5, we show the general trends of $\rho(h)$ (in black), $V(h)$ for three cases, in green, brown and blue curves marked by V_1 , V_2 and V_3 respectively and $\rho(h)V(h)$ for the same three cases (not marked for clarity). In all the cases, there is a height where the lift is maximum. Actual height depends on balloon material. In Fig. 6, we show this lift once more for a single case where the height is plotted vertically. In Fig. 7 this is shown for two balloons B_1 (blue) and B_2 (green) which are tied together. There could be two situations: In the first case (top), the net lift $L = L_1 + L_2$ is much higher compared to the payload mass M_p (as each of the lifts L_1 and L_2 is higher than the payload mass M_p) and at a break altitude h_{b2} one balloon, say B_2 (green), bursts and B_1 has to carry the payload alone till its lift is the same as M_p and the balloon reached neutrality at an equilibrium altitude h_e . With decrease in temperature at nightfall the lift is reduced and system descends through the maximum lift point to the ground. In the second case (bottom), individual lifts are very low, but the highest lift point still crosses the mass of the payload M_p . In this case, the equilibrium height is very low, and it descends even as the temperature is reduced slightly (e.g., by the sun set).

3 Payload description

The payload of a typical mission includes a Main Measurement Unit (MMU) which, for example, could be a scintillator type detector or Geiger-Müller (GM) counter. The MMU must be supported by some other essential/optional ancillary equipments like Attitude Measurement Unit (AMU), Video Camera Unit (VCU), Sun Sensor (SS) and Global Positioning System (GPS) Unit (GPSU). Tracking and recovery of the payload is handled by Positional Information Transmission Unit (PITU) and/or simply Position Alert System Unit (PASU) using cellphone network (GSM communication) which is automatically activated upon landing when it is under GSM network coverage. The payload units and their components along with their purposes are summarized in Table 1. The Power Supply Units (PSU) consist of a stack of rechargeable batteries and are generally Li-Po type. Instead of a centrally powered system, we put several such units to increase the chance of receiving some data in case of failure of some PSUs.

The SS normal axis and AMU sensor z axis are always parallel to the MMU z axis (i.e., normal to the detection surface) so that both can see the same object. The orientation of the video camera or cameras may vary depending on the purpose of observation. The MMU detector is generally attached to the top lid of the payload container for clear access of all electronics and battery inside the container.

The overall payload orientation depends on the observation goal we are interested in and varies with the position of the target object in the sky during the mission flight and we fix the tilt angle of the payload accordingly when we suspend the payload from the balloon.

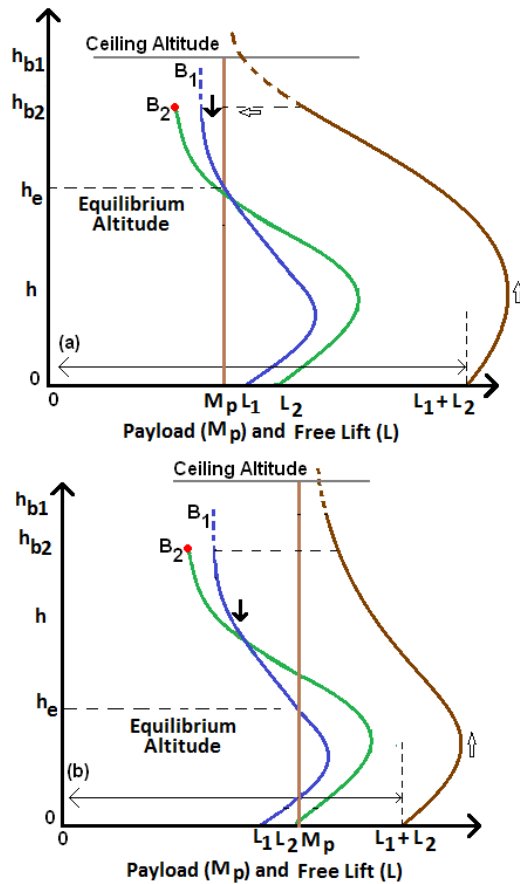


Fig. 7 Example of the cases when it is possible to have a neutral buoyancy when a single balloon bursts and the other remains intact in a double-balloon configuration. (top) When both balloons have lifts much higher than the payload weight. (bottom) When the lifts are comparable or less than the payload weight, such as when the payload is massive. See text for details.

The GPS and GSM antenna are always on the top lid of the payload container or at the side depending on the payload tilt angle so that it can see the sky to be able to receive GPS satellite data. In Fig 8 we present a typical payload as seen from outside (top). We also show the arrangements of the main instrument along with the ancillary instruments with the lid open (bottom).

3.1 Main measurement unit

In ICSP balloon experiments our main goal has been the temporal and spectral study of high energy radiation, be it from cosmic rays or solar or other extra-terrestrial objects. We therefore keep an X-ray detector as the main detector in the payload. This can be changed according to the need. Considering the goal of our experiment and

Unit	Component	Purpose
MMU	Scintillator (2" or 3" NaI, 5" CsI/NaI Phoswich)	Spectral and temporal X-ray and cosmic ray measurement.
	GM counter	Temporal X-ray and cosmic ray measurement.
AMU	9DOF, P-T sensors	Payload attitude measurement in terms of altitude and azimuth angle, also includes pressure and temperature measurements.
VCU	HD video camera	Optical movie and/or image of the sky, ground/ carrier balloons/meteorites/sun and planets.
SS	Photo sensor	To cross-check if the Sun is inside the detector FoV.
GPSU	GPS receiver	Record the flight path using GPS satellites.
PASU	GPS tracker	Send location upon landing using GSM network.
PITU	Wireless transmitter	Send on flight positional information recursively in predefined time interval.

Table 1 Payload components and their purpose.

constraints on energy range, mechanical robustness required for the mission, weight limitations etc., we chose scintillator detectors as the candidate. Sometimes to measure the secondary CR events in the atmosphere we use GM counters as the MMU on board the mission (see, Chakrabarti et al. 2011). This measurement unit consists of two main parts: X-ray detector unit and readout electronics unit to record the events from the detector. We discuss these parts in more detail along with other parts such as collimator, power supply etc. in the following Section.

3.1.1 Scintillator detector

The scintillator detector consists of a scintillating crystal optically mounted on a Photo-Multiplier Tube (PMT) for the Primary readout of the energy deposition. Due to efficient energy absorption mechanism, Sodium Iodide (NaI) and Cesium Iodide (CsI) have been the most useful inorganic scintillator material for hard X-rays. NaI yields more light and consequently better energy resolution, though it should be handled more carefully during the packaging since it is extremely hygroscopic. We use a NaI(Tl) (and in some cases CsI(Na)) crystal hermetically sealed in an aluminum housing to prevent the crystal quality deterioration.

The PMT is optically coupled directly to the scintillator crystal. The PMT is guarded by a mu-metal magnetic shield. The scintillator container and mu-metal shield are sealed together to form a low-mass and light-tight housing for the detector.

The working energy range of the detector depends on the energy deposition efficiency of the crystal which depends on the crystal material as well as on its dimension.

We used detectors with different crystal sizes mounted on a suitable PMT according to the mission purpose(s). We mostly used cylindrical crystals of NaI(Tl) and in some cases CsI(Na). Apart from these single crystal scintillator detectors, sometimes we also used Phoswich detectors where two different kinds of crystals (viz. NaI(Tl) and CsI(Na)) are optically coupled together with a single PMT. This type of scintillator detector is used for better background subtraction and better spectral data. A list of detectors with their specifications is given in Table 2.

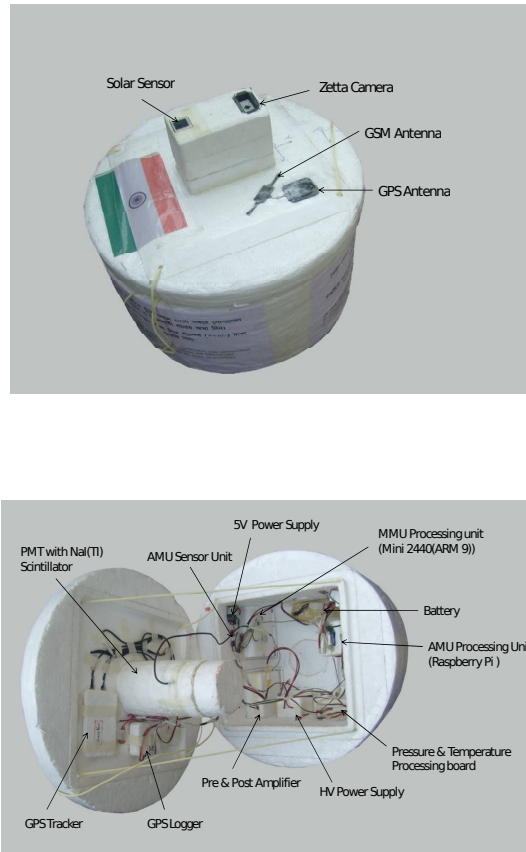


Fig. 8 Overall view of a typical payload (top) and the internal placements of the main instrument and other components (bottom).

Detector	Crystal material	Thickness (cm)	Diameter (cm)	Weight (with PMT)(g)
Bicron 2M2/2	NaI	5.08	5.08	900
Bicron 3M3/3	NaI	7.62	7.62	1900
Harsaw (3")	NaI	7.62	7.62	2100
Philips (5")	CsI	0.6	11.60	1050
Phoswich (5")	NaI + CsI	0.3 (NaI), 2.5 (CsI)	11.60	2700

Table 2 Properties of the scintillators (NaI(Tl) and CsI(Na)) crystals used in different missions.

The electronics readout system in the detector module consists of: (i) front-end electronics with signal amplifiers, (ii) electronics for event pulse generator (triggering circuit), (iii) peak hold electronics, (iv) digitization and on board storage system and (v) high voltage DC-DC converter power supply.

Fig. 9 shows the block diagram of the whole scheme of the signal readout system and the scintillator detector assembly.

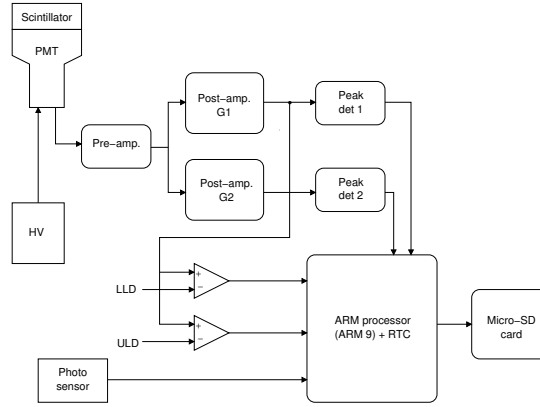


Fig. 9 Schematic block diagram of the scintillator detector assembly.

Post-amplifier amplifies the pre-amplifier output pulses without affecting the pulse shape (i.e., decay time). It also provides low impedance to the following processing and analyzing circuit. Though we are generally interested in the energy range of $\sim 15 - 150$ keV, still sometimes we are also interested in higher energy phenomena (such as terrestrial gamma ray flash or TGF) and for this reason, in our circuit we have the provision to read up to ~ 2000 keV. This large range of energy band cannot be handled by a single amplifier without sacrificing the energy resolution. So, as shown in Fig. 9 we use two post-amplifiers: one of high gain (G1) for the energy range $\sim 15 - 150$ keV and another (G2) for $\sim 100 - 2000$ keV, a low gain amplifier.

We generally operate the detector in the event mode, i.e., we record each event with its pulse height and arrival time information, with a 1 ms resolution in the time stamp. Since we do not transmit scientific data, we have no limitation on the data acquisition amount. We store the data on board. This is a clear advantage over data storage process in satellite observations as the latter depends on the downlinking rate.

The primary energy range of our detector, according to our scientific goal covers the range from $\sim 15 - 150$ keV where we expect to observe the X-ray emissions from point like sources. To reduce the background counts we need to use a collimator. The FoV of the collimator depends on our observation purpose and also on the constraint on the payload weight. Since we do not have any provision of pointing the payload to a fixed object, the payload will rotate at different rates at a different height and not necessarily always in the same sense. Thus in order to detect a specific target for a considerable amount of time, the FoV should not be too narrow. Considering these constraints we generally use 0.5 mm lead sheets in different configurations to build the collimator. Use of 0.5 mm lead collimate effectively $\sim 95\%$ up to 100 keV. The use of lead as the collimator has a problem at around 75 keV due to its K_α emission line, this can be, up to some extent, corrected during the analysis of the data by subtracting the line. In some of the missions we desire more precise spectral

data. For these we designed the collimator with 1.0 mm tin sheet along with 0.25 mm copper (to absorb the K_{α} line emitted from tin).

The energy range allows us to study low energy radiations from the sun and compact objects, as well as the secondary cosmic rays. Above ~ 100 keV our detectors become collimator-less due to the transparency. So events such as gamma ray bursts or ubiquitous electron-positron annihilation lines could be seen without any problem. The lead emission line or the annihilation line can be used as calibrators, though we often use other calibrators on board as well.

3.1.2 Geiger-Müller counter

Different kinds of GM counters were used mainly for the purpose of measuring the secondary CR in the atmosphere. One kind of these is a 4.9 cm long and 1.5 cm diameter Ne+Halogen filled cylindrical GM counter with stainless steel body and a Mica window at one end. The other kind of GM counter is a 10.1 cm long and 1.1 cm diameter stainless steel tube filled with Ne+Halogen with no window. Sometimes we used several of these second kind of GM counter together to increase the effective detection area. These GM counters were used to count the secondary radiation in the atmosphere using suitable readout electronics. A schematic block diagram of the detector set up using GM counters is shown in Fig. 10. These counters inside a 1cm lead tube were used also to measure atmospheric muons (e.g., Chakrabarti et al. 2013).

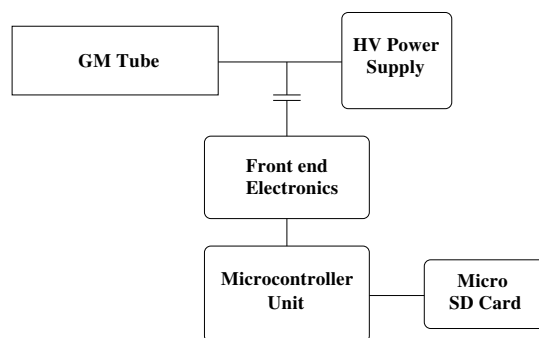


Fig. 10 Schematic block diagram of the GM counter assembly.

3.2 Ancillary equipments

3.2.1 Video unit

Along with the purpose of capturing the extraterrestrial objects like Sun, moon, bright stars and planets, meteorites etc., the video camera unit can capture an excellent areal view of the Earth from various altitudes. The unit acts as a visual monitor of the total

mission, provides crucial information about how the size of the balloons change with height, provides exact moments of launching of payloads, balloon bursts and landing of the payloads apart from possible reason for entanglements between the balloon and the payload, if any, during the descend.

3.2.2 Sun Sensor

Especially, for the solar X-ray observation we use a Sun sensor device to cross-check if the sun was indeed in the field of view when the data in MMU is sorted out as coming from the sun. For this purpose, we use a photo-sensor to capture the optical photons from the Sun. The FoV of the Sun sensor is kept to be the same as the FoV of the detector in the MMU by using suitable collimator and aligning the axes of the two instruments.

To make the sensors light weight, the collimators are made from a black cardboard roll held tight with duct tapes to provide mechanical strength. The photon intensity from the Sun at higher altitudes during the mission flight gets higher when scattering of the lights becomes small due to rarefied atmospheric medium. This saturates the photosensor. To reduce the photon intensity, filters are used in front of the sensor. Filters made of two 2.5 mm thick black acrylic sheet are enough for this purpose.

3.2.3 GPS unit

GPS is one of the most important modules used to obtain instantaneous payload location (attitude, longitude and altitude) and the wind parameters at different levels through the atmosphere. The payload location information is very important for the later use during the data analysis as well as to track the payload for its recovery.

The GPS module used in the payload has a form factor of 19.0×27.0 mm and is of light weight. This module is connected with an external antenna. The receiver uses a patch antenna and provides serial data output. The power consumption by the module is also negligible.

3.2.4 Payload attitude measurement unit

Due to the limitation on the payload weight it is not possible to include a conventional pointing device in the payload for continuous observation of any specific target. Instead, we use a device to measure the payload attitude with time, so that later during the analysis of the data we can extract the instantaneous direction of the detector. We use Inertia Measurement Unit (IMU) sensors for this purpose. The data from these sensors are processed by a processor board and stored in the memory for future analysis.

The main components of the AMU are as follows:

- One three axis Accelerometer
- One three axis Magnetometer
- One three axis Gyroscope

The 3-axis accelerometer provides the linear acceleration along its three axes. The acceleration due to gravity (g) can be used as the reference to calculate the tilt angle of the device with respect to earth. This is employed in calculating the two Euler's angles: the roll and pitch.

The 3-axis Magnetometer provides components of the Earth's magnetic field magnitude along its axes. This parameter is essential in computing the heading angle for the payload.

The 3-axis gyroscope provides the angular rate around its each axis. The accelerometer and the gyroscope together are used for sensor fusion and calculation of exact roll and pitch angles. The pitch and the roll angle data is then used for tilt-compensating the Magnetometer for accurate heading angle calculation. However, bias, hard-iron and soft-iron calibrations are performed prior to tilt-compensation during the ground test and calibration. During the flight operation we only record the data from the sensors for all the axes and store them with proper time tag. During data analysis we extract the pitch, roll and yaw angle information of the payload using these data for a particular time and consecutive altitude and azimuth (or, RA/DEC) of the detector viewing direction.

The IMU sensor stick is connected to the Raspberry Pi processor board which is the main computing unit here. This board gets the time information from an external RTC module. Additionally, this board acquires other house keeping data like pressure, temperature and location data from the pressure/temperature sensors and GPS module. All these information are processed in sub-second time interval and stored in an external SD card.

3.2.5 Pressure and temperature measurement unit

We use two temperature sensors and one pressure sensor in our payload. The pressure sensor and one temperature sensor are installed outside the sealed payload box to measure atmospheric temperature and pressure and one temperature sensor is used inside the box to monitor the temperature of the motherboard inside. The pressure sensor is a piezoresistive material which when subjected to some mechanical force provides a response in terms of voltage change. Here, the force is exerted by air on the piezo diaphragm of the sensor. The sensor produces its response which is an analog quantity and fed to an analog to digital converter to convert it into a form which the on board computer understands. The digitized data is then stored to a solid state storage media on board. The temperature sensor used is an integrated circuit. It provides a change in current flow through it when subjected to temperature change. A series resistor is employed with the transducer to convert the current into a voltage which is fed to an ADC and then saved in the storage media by the on board computing unit. The calibration of the sensors is done in our lab with our setup.

Figure 11 gives a schematic diagram of how we combine data from various units and store on board.

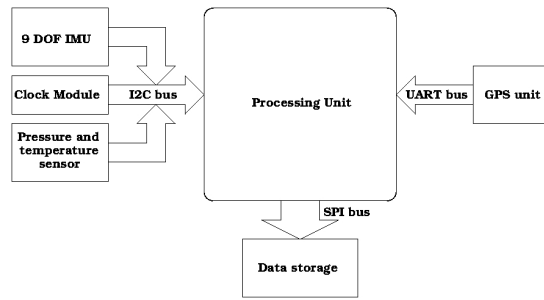


Fig. 11 Schematic diagram of all the ancillary units used on board a typical payload.

3.2.6 Positional Information Transmission Unit

The recovery of the payload largely depends on the anticipation of its landing location and on-the-go tracking features used in the mission. For this purpose we designed a light weight and rugged device which can give the real time positional information of a payload on board the carrier to the mobile ground base. This live data of the payload location helps us to track the current position of the payload and also to optimize the prediction of the landing location.

The Positional Information Transmission Unit (PITU) on board in the payload along with its receiving part in the mobile ground base comprise the payload tracking system.

The transmitter unit in the payload consists mainly of three parts: GPS information receiving unit, computing unit and the Transmitter. The GPS information is read in the system from the GPS module. A micro-controller is used to implement the functionalities like parsing, preparation of the data packet in proper format, synthesizing the signal data, transmitting the data to the antenna via an amplifier. The whole part is implemented in firmware of the micro-controller. We use standard short range two way devices which are generally used for voice communication at the RF transmitter. The micro-controller modulates the data with the two generated tones of 2200 Hz and 1200 Hz. These modulated signals are transmitted from the payload to the ground. At the ground station, the receiver tuned to the same channel, receives and feeds the output to a standard sound card of PC/laptop to digitize the analog signal. For meaningful decoding of the received data, many publicly available packet radio decoder software are available. This software unit decodes the signal packets. There are also provisions where one can directly use the data over a calibrated map (such as the Google map) to get the instantaneous position of the payload in the sky. There is also a provision to log the data. The data obtained as the balloon goes up is used for predicting an estimated landing location with an estimated landing path of the payload after balloon bursts. Of course, in case we miss some data in transmission due to signal weakness, we can get the full data set from the GPS unit on board after payload recovery.

The requirement of the payload recovery has led us to implement another module in the payload: Position Alert System Unit (PASU) to send the final location of the payload upon landing. For this system we use a GSM/GPRS/GPS Tracker device

which are commercially available in the market (used for the purpose of vehicle tracking, for example). This device works using existing GSM/GPRS network and GPS satellites and is able to locate or monitor the remote target by SMS or internet. It uses GPS, GSM dual position information and automatically stores the GPS location information when the GSM signal is bad. This is a very compact and light-weight module (dimension $64 \times 46 \times 17 \text{ mm}^3$ and weights only 50 g), uses GSM/GPRS network for communication (using 850/900/1800/1900 MHz band). The position accuracy is up to 5 m, so upon receiving the landing coordinates through SMS we can reach the exact position to recover the payload. The power required by this device is very nominal and is supplied from the main power supply of the payload. PASU sends out an SMS with the location information of the payload to the caller when it is in contact with a cellphone network.

4 Test, calibration and responses

4.1 Tests in Atmospheric simulator

During the flight, the detector undergoes a reasonable amount of pressure and temperature change and we are restricted to use no pressure container or better temperature shielding due to the weight limit on the payload. In order to test that the sensor would perform during the flight as per specifications, we need to test the detector and other payload components under such simulated environment. This enables us to calibrate the performance with varying atmospheric conditions.

For the testing of the payload components under temperature variation we use a temperature simulation chamber where in a encapsulated vessel we gradually bring the temperature down (to about -10°C) from room temperature. The pressure variation may affect the detector for any mechanical deformation which may lead to the gain change of the detector. Another crucial effect is on the electronics part especially on the high voltage biasing of the detector due to the change of dielectric constant of the medium. Though we use a potting material surrounding the high voltage bias part to prevent this effect, we still need to test the system under low pressure condition. For this purpose, we have a test bench containing an air-tight glass container fitted with suction pump. This system can bring the pressure down to about 6 – 7 mbar which corresponds to about 35 km height in the atmosphere. At this pressure value the detector and other payload components show no deviation in performance.

4.2 Detector calibration

We have the detector data with a time resolution of 1 ms and the whole energy range is recorded in 1024 channels. For calibration of the detector's energy response we use Eu^{152} , Ba^{133} and Am^{241} radiation sources which have 5 lines inside our energy range (39.5 keV and 121.9 keV for Eu, 30.9 keV and 81.0 keV for Ba and 59.5 keV for Am). Fitting of these lines gives us a linear channel to energy relation. We also calculate the energy dependance of the detector resolution which is useful for spectral analysis of the data obtained from the detector. The payload on board generally

requires no calibrator since we have two natural ones: the emission line (at ~ 75 keV) from the lead collimator as well as the 511 keV lines in high channels.

4.3 Detector and atmospheric response calculation

The balloons can take the payloads up to about 35 – 42 km. During the course, the detectors gather extraterrestrial X-ray data which have to pass varying amount of residual atmosphere and hence suffer variable absorption effects. So to trace back the original spectra of the X-ray data it is necessary to calculate the absorbing nature of the varying residual atmosphere. This can be done by means of the simulation with a proper atmospheric model.

For this purpose, we consider the NRLMSISE-00 atmospheric model (*Picone et al.*, 2002) to construct the geometry of the atmosphere. We simulate the propagation of the photons and other charged particles through the atmospheric model by using Geant4 simulation toolkit (*Agostinelli et al.*, 2003).

Similarly Geant4 toolkit is also used for the simulation of the detector response. We calculate the total detector response for the detectors with the shielding and the collimator due to the incident photon energy from 10 keV to 1 MeV. This response on the other hand will depend on the direction of the incident photons due to the presence of the collimator, shielding material and geometry of the detector. So we simulate the response of the detector for the photon in two directions: parallel photon beams through the collimator aperture and isotropic distribution of photons from the upper hemisphere of the detector coming into the detector.

We also calculated the detector response for other major charged particles in the atmospheric region of our interest which is also necessary to understand the data from the detectors and as well as to extract the X-ray data from the background. The detailed procedure will be discussed elsewhere.

5 Results and discussions

We now present a few samples of our results to show the capabilities of our low-cost missions. In all our missions, we turn on the instruments one after another before the lift-off carefully recording each of the turn-on times in order to synchronize the data during analysis. They are turned off after descend. Thus, we always get the cosmic ray data in all our missions and large on board storage allows us to store this data for the entire trip.

5.1 Results from peripheral instruments

First, we give two frames of a video taken from the payload in Fig. 12. On the left, we present a photo of the Earth from a height of ~ 40 km. On the right, we show the moment one balloon is shredded at its burst height. The other balloon remains intact.

As discussed before, the variation of altitude with time depends strongly on the lifts given at the time of launching and the combination of balloons. In our experience

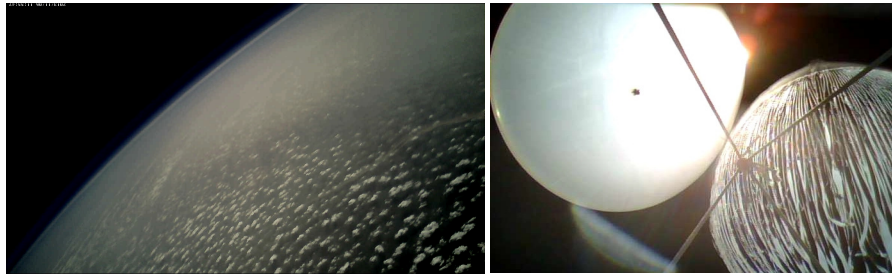


Fig. 12 (left) A snapshot of the Earth from a payload at a height of ~ 40 km. (right) Burst of one of the two rubber balloons while the other remains intact due to lower lift given at the launching.

of launching 101 Dignity Missions (D1 to D101), we have come across mainly five types of profiles four of which are given in Fig. 13 and the fifth with some description is given in Fig. 14. In Fig. 13(a), we show a typical (Dignity 75 or D75 mission) single time-altitude profile where the payload steadily reaches the burst height with almost constant vertical velocity. Right after the burst, the payload falls almost freely to a height of about 20km and then as the parachute becomes steady, the landing is slower. In Fig. 13(b), taken from D90 mission, we see slower descend from the very beginning. Here, one balloon bursts, but the heavy payload continues to descend due to lower lift of the remaining balloon. In Fig. 13(c), taken from D52 which was launched at a winter night, the payload height is saturated as the balloons shrink at lower temperature of the stratosphere. At the sun rise, they went up a bit till one bursts and the other brought the payload down. In Fig. 13 (d), taken from D92 where a polythene balloon was used, the ascending, descending as well as the behaviour above ~ 30 km are different from those of rubber balloons. We note that the peak is blunt as the balloon continues to rise even when it is torn apart at places. The descend is smoother as well.

In Fig. 14, the time height profile during D59 mission is shown where the effect of near neutrality due to burst of a single balloon is demonstrated. During the ascending phase, the velocity was almost constant. After the burst of one balloon, the other brings the payload down to an altitude of about 20km and floats at neutral height till evening sets in at Indian Standard Time (IST) ~ 64000 s when the balloon shrinks and the lift is reduced. This finally brings the payload down to the ground slowly. In one of the Missions (D26) we achieved the mission duration of about 12 hours in this process.

The most important aspect of our Missions is the recovery of the payload, as the scientific data is on board and the budget is limited. So, it is extremely important that we reach the landing site as the payload lands. For this purpose, prediction of the payload trajectory with appropriate input parameters and the selection of lifts, parachutes (to manipulate the descend rate) etc. before the mission is very crucial. We generally have a good predictability rate. Very often we see the descend of the parachute (Fig. 3 in D17). A comparison of the predicted and real trajectory of a mission for D91 is shown in Fig. 15.

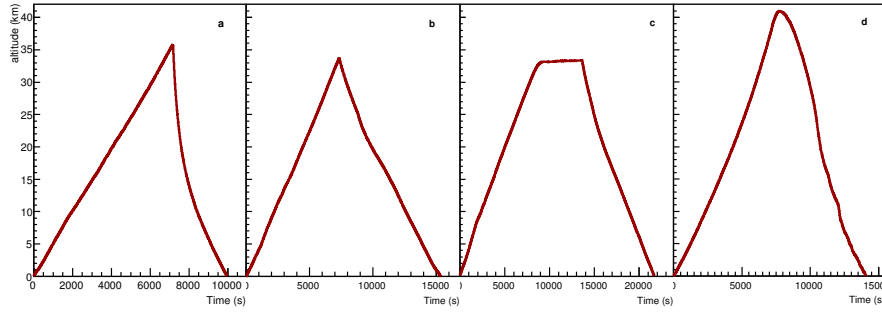


Fig. 13 Payload altitude profile with time for various carrier modes (D75/90/52/92). (a) A single rubber balloon, (b) Two rubber balloons with heavier payload, (c) A night flight with two rubber balloons, (d) A single polythene balloon.

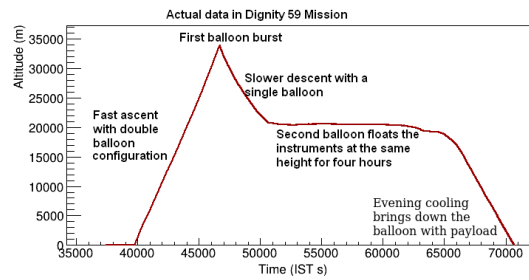


Fig. 14 Time height profile during D59 mission. Near neutrality is achieved at a height of about 20 km after a balloon burst.

In all our missions, we obtain the atmospheric parameters, such as the pressure and temperature outside the payload box. These parameters are important to check the working environment of the detector. However, our data could be very useful for meteorological purposes as we reach heights of 40 km or more. The variation of pressure and temperatures with altitude is shown in Fig. 16.

Measurement of wind velocity at different altitudes is important in the atmospheric study as well. Components of wind velocity is a byproduct from all our missions. We can retrieve the wind velocity profile up to a very high altitude which is not generally done in the regular atmospheric studies. As an example, we present the profile of the wind velocity in south-north and west-east directions at different altitudes as shown in Fig. 17.

Depending on the target source, the payload is tilted at an angle with vertical axis. However, the azimuthal angle is not known a priori. So, the information of the payload orientation is important to know the direction from which photons are entering into our instruments. This enables us to locate the position of X-ray sources in the sky. We calculate the detector axis direction using the data of the AMU installed in the payload box. In Fig. 18 we show the direction of the detector axis in horizontal coordinate system.

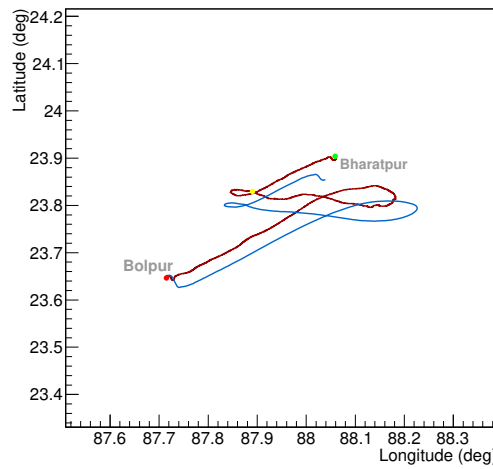


Fig. 15 Comparison of the predicted and real flight trajectories plotted on a google map of the region. The predicted data (blue) is taken from the online flight path predictor before the mission with appropriate input parameters and the real data (red) from the Mission GPS data.

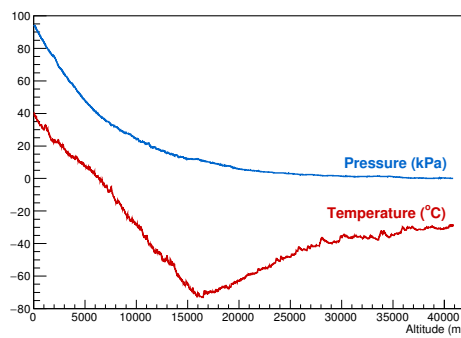


Fig. 16 Atmospheric pressure and temperature profile with altitude in D97 Mission. The atmospheric temperature (in °C) external to the payload is shown by red and the atmospheric pressure (in kPa) is in blue.

Normally a single balloon flight lasts of about three hours. However, when a double balloon is launched, depending on the distribution of the lifts and the mass of the payload, the duration could be very long, perhaps 12 hours or longer. One such mission parameters are shown in Fig. 19 where we show the altitude variation in blue, the pressure variation (kPa) in cyan and the IMU data (acceleration in x-direction) in green. Note that the payload floated for almost five hours at about a constant height of 22 km. Note also the IMU parameter indicating the burst of a single balloon (spike at ~ 20000 s) and some turbulence thereafter till the neutrality height is reached.

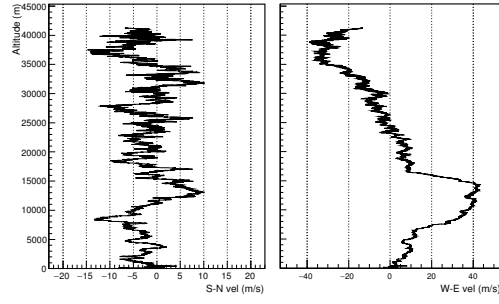


Fig. 17 Wind velocity profile in the south-north and west-east directions at different altitudes up to more than 40 km in D101.

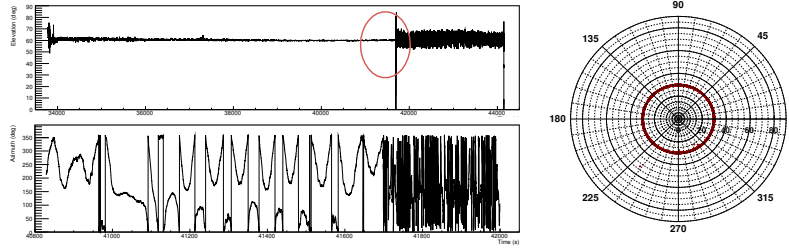


Fig. 18 Payload attitude information obtained from the IMU in D98. Two panels on the left show elevation (top panel) and azimuth angles (bottom panel) around the burst time marked by an ellipse of the detector direction (axis of the MMU). On the right we show the annular part of the sky covered by the detector direction vector (red points) above 30 km altitude till burst.

5.2 Scientific data

We now turn our attention to obtain samples of scientific data from our low cost Dignity Missions. We present results of Cosmic Rays, Solar flares electron-positron lines just to indicate the data quality. Detailed data analysis of specific missions would be presented elsewhere.

5.2.1 Cosmic Rays

The interaction of the primary CR with the atmospheric nuclei produces secondary cosmic-ray shower (*Grieder, 2001; Gaisser, 1990*). Our detector is capable of detecting low energy X-ray part of these secondary products. Intensity of the secondary X-ray depends on the altitude as the atmospheric density and composition varies with altitude. The interaction of the primary CR gradually intensifies at lower heights producing more secondary particles. But the loss effect due to absorption and decay processes also become more at lower heights as the density gets higher. Due to the balance of these interactions we get a maximum secondary intensity around 15 – 20 km depending on the geomagnetic latitude of the location (*Bazilevskaya and Svirzevskaya, 1998; Harrison et al., 2014; Li et al., 2007; Schönfelder et al., 1977;*

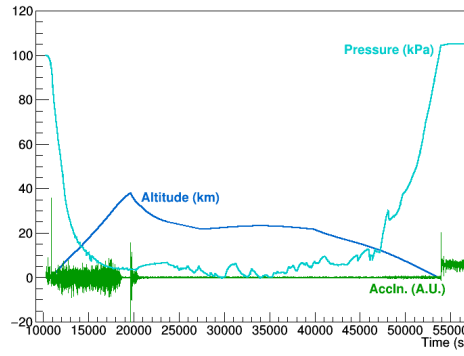


Fig. 19 Pressure, Altitude and acceleration data of D26 mission showing a 12 hour flight duration in a double balloon launch.

Yaniv et al., 2016). In Fig. 20 we have shown the spectral change of the secondary CR dynamically with altitude.

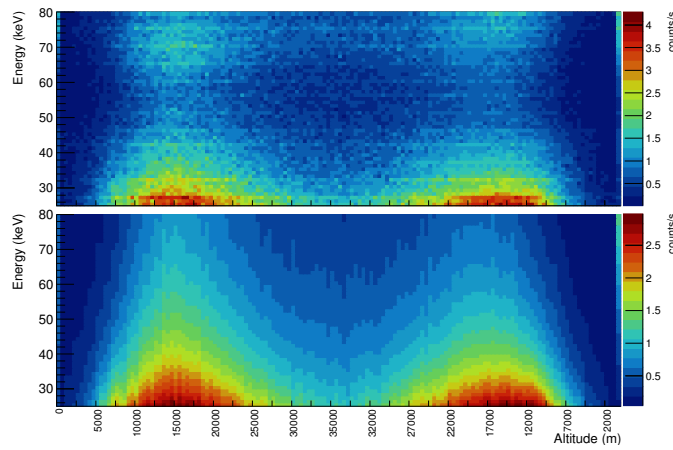


Fig. 20 Dynamic spectrum of the secondary CR with altitude. The upper panel shows the detector data including emission effect from the lead collimator shielding. Lower panel data shows the result after removing the emission effect.

The secondary cosmic ray spectrum due to the interaction of primary cosmic rays in the atmosphere near the Pfozter maximum is shown in Fig. 21. This spectrum shows a power law distribution of the form $931.7 \times E^{-1.73}$ shown by the fitted solid line along with the spectrum.

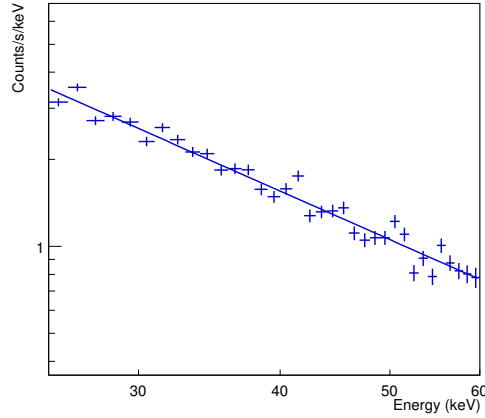


Fig. 21 Spectrum of the secondary CR near the Pfozter maximum. Solid line is the best fit power-law curve for the spectrum.

5.2.2 Solar flare

Since the Sun is the most X-ray bright extraterrestrial object in the sky, we targeted it in several missions, especially during flare times. Our mission preparedness allows us to prepare and launch as soon as the Sun becomes active. Only delay arises from the Airport Traffic Controller's permission to fly. Thus we have a good amount of data from the quiet and the active sun. Fig. 22 shows the light curves in 42 – 70 keV (black) during a solar flare. The Sun entered inside our FoV (35°) of the $2'' \times 2''$ NaI(Tl) Bicron detector (*Saint-Gobain Crystals*, 2016) after the payload ascended above the height of the Pfozter maximum. We plot the low energy (3 – 25 keV) light curve of NASA GOES satellite (*Space Weather Prediction Center*, 2015) also on the same plot (red). We lost the low energy data due to heavy absorption below Pfozter maximum. Our light curve generally follows the GOES light curve. However, high energy emission (*Krucker et al.*, 2008) is always of shorter time duration as we find here also. Lower intensity superposed GOES flaring events could not be detected at higher energy channels in our observation. This light curve is not corrected for changes in atmospheric absorption with height.

5.2.3 $e^- - e^+$ annihilation lines

Primary and secondary cosmic rays impinging on the collimator or nearby metal casings will produce copious charge particles. Most importantly, electrons and positrons annihilating nearby are picked up by our detector and its strength is directly related to the secondary radiation intensity. In Fig. 23, left panel, we present the dynamic spectrum at very high energy (200 - 1600 keV) as a function of the altitude. The Pfozter maximum can be seen at about ~ 16.5 km. The $e^- - e^+$ annihilation line at 511 keV could be seen very clearly. The intensity of the line is proportional to the radiation content in the surroundings. At about 40 km, the secondary radiation is very low and

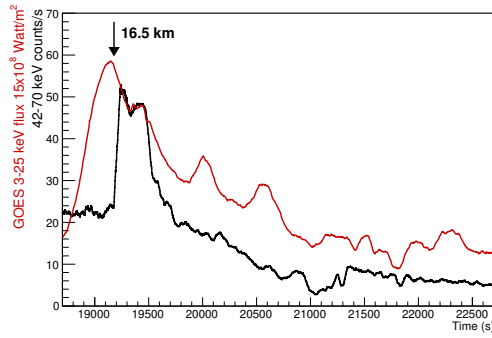


Fig. 22 Solar light curves in 42 – 70 keV (black) showing the high energy detection of a solar flare during D40 mission on May 18, 2013 by a scintillator detector of $2'' \times 2''$ NaI crystal. The 3 – 25 keV solar flux data from GOES satellite also detected the same flare.

therefore this line intensity is also reduced. In the right panel, we plot the spectrum only at the Pfofzer maximum. The sharp line could be seen.

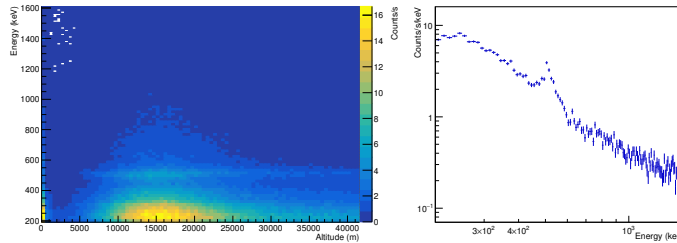


Fig. 23 (Left) Dynamical spectrum of secondary Cosmic Rays in high energy channels in D101 showing Pfofzer maximum at around 16.5km. We also see the $e^- - e^+$ annihilation line at 511keV. (right) Spectrum at the Pfofzer maximum showing clearly the annihilation line.

6 Conclusions

In this paper, we discussed a new paradigm of near space exploration where one can carry out sophisticated space based observations using very low cost rubber and small polythene balloons which are commonly used for meteorological purposes. The light weight payloads contain both the main measurement unit with on board data storage, as well as ancillary units such as GPS data transmitter, inertial measurement units, video cameras, sun sensors etc. Power is supplied from rechargeable Li-Po type batteries. We concentrate on the X-ray sky, namely, the cosmic rays, the Sun and the compact objects. Duration of each mission could be between 3 to 12 hours. Because of event mode data storage, we can save time stamps of each received photon. Inertia measurement unit enables us to tag each photon with the directional information from

which each photon is received. That way, even if we have no pointing device, we can separate photons from each source. We have shown that we have been able to obtain dynamical spectrum of cosmic rays, solar flares, and even electron-positron annihilation lines have been detected quite prominently. We have presented wind and atmospheric parameters. In our double-balloon approach, we have been able to achieve a remarkable feat to float a payload at near constant height for hours by suitably manipulating the lifts of the balloons. We have presented qualitative pictures of how this could come about.

Though there are many limitations of our low cost flights, we also have several advantages which are not easily achieved by more expensive methods. For instance, we have Cosmic ray variation data year after year which appears to be anti-correlated with solar activity (Sarkar *et al.*, 2017). Because payloads are very light, we have taken many innovative approaches at each stage. The recurring cost is so low, effectively the cost of the balloons and the gas along with logistics, that younger generations can have access to serious space research. Our method is also applicable for testing small payloads in preparation for future space missions. It is also useful to assess radiation hazards and aviation safety (Miroshnichenko, 2003; Radiation exposure prediction, 2016).

Our main goal in the paper was not to present specific results, but to impress what could be achieved, in principle. In separate papers, we will discuss in details of how X-ray spectra of the Sun, or pulsar or black hole candidates could be obtained or the secondary Cosmic rays could be monitored. We have procured an wealth of information about the pattern of atmospheric parameters including pressure, temperature and winds before and after the Indian monsoon year after year. These will be valuable for weather prediction.

Acknowledgements The authors would like to thank Dr. S. Mondal, Mr. S. Chakraborty, Mr. S. Midya, Mr. H. Roy, Mr. R. C. Das, Dr. S. Chakrabarti and Mr. U. Sardar for their valuable help in various forms during the mission operations and data collection. We also thank Ministry of Earth Sciences (Government of India) for partial financial support.

References

- Agostinelli, S. et al.: Geant4 - a simulation toolkit. *Nuclear Instruments and Methods in Physics Research*, A 506 250-30, (2003)
- Bazilevskaya, G. A., and Svirzevskaya, A. K.: On the stratospheric measurements of cosmic rays. *SpScR* 85, 431–521, (1998).
- Chakrabarti, S. K., Bhowmick, D., Sarkar, R., Mondal, S., Sen, A.: High Energy Astrophysics with Rubber Balloons. European Rocket and Balloon Programme (SP-700), p. 581 (ESA:Netherland) (2011).
- Chakrabarti, S. K., Bhowmick, D., Palit, S., Chakraborty, S., Mondal, S., Bhat-tacharyya, A., Midya, S., Chakrabarti, S., A New Paradigm in Space Based Experiments Using Rubber Balloons (SP-721), p. 663 (ESA:Netherland) (2013).
- Chakrabarti, S. K., Bhowmick, D., Chakraborty, S., Palit, S., Mondal, S. K., Bhat-tacharyya, A., Midya, S., Chakrabarti, S.: Study of properties of cosmic rays and solar X-ray flares by balloon borne experiments. *IJP* 88, 333–341, (2014).

- Chakrabarti, S. K., Bhowmick, D., Sarkar, R., Bhattacharyya, A., Midya, S., Unique High Energy Experiment Initiative by ICSP with Weather Balloons, (SP-730), p. 557 (ESA:Netherland) (2015).
- Cambridge University Space Flight Landing Predictor. <http://predict.habhub.org>, (2016). Accessed 19 Nov, 2016.
- Gaissner, T. K.: Cosmic Rays and Particle Physics. *Cambridge University Press*, (1990).
- Grieder, P. K. F.: Cosmic Rays at Earth: Researcher's Reference Manual and Data Book. *Elsevier Science*, (2001).
- Harrison, R. G., Nicoll, K. A., Aplin, K. L. 2014, Vertical profile measurements of lower troposphere ionisation. *JASTP*, 119, 203–210, (2014).
- Krucker, S. et al.: Hard X-ray emission from the Solar corona. *A&A Rev.* 16, 155–208, (2008).
- Li, S. W., Li, Y. S., & Tsui, K. C.: Radioactivity in the atmosphere over Hong Kong. *JEnRa*, 94, 98–106, (2007).
- Miroshnichenko, L. I.: Radiation hazard in space. *Springer-Science+Business Media*, (2003).
- Picone, J. M., Hedin, A. E., Drob, D. P., and Aikin, A. C.: NRL-MSISE-00 Empirical Model of the Atmosphere: Statistical Comparisons and Scientific Issues. *JGR*, 107, A12, 1468, (2002)
- Radiation exposure prediction. <http://csp.res.in/ICSP-WEB/xrayfiles/xray.html>, (2016). Accessed 28 Aug. 2016.
- Saint-Gobain Crystals. <http://www.crystals.saint-gobain.com>, (2016). Accessed 28 Aug. 2016.
- Sarkar, R., Chakrabarti, S.K., Pal, P.S., Bhowmick, D. and Bhattacharyya, A.: Measurement of secondary cosmic ray intensity at Regener-Pfotzer height using low-cost weather balloons and its correlation with solar activity. *AdSpRes*, doi:10.1016/j.asr.2017.05.014 (2017)
- Schönfelder, V., Graser, U., and Daugherty, J.: Diffuse cosmic and atmospheric MeV gamma radiation from balloon observations. *ApJ* 217, 306–319, (1977).
- Space Weather Prediction Center. <http://www.swpc.noaa.gov>, (2015). Accessed 30 Aug. 2015.
- Yaniv, R., Yair, Y., Price, C., Nicoll, K., Harrison, G., Artamonov, A., Usoskin, I.: Balloon measurements of the vertical ionization profile over southern Israel and comparison to mid-latitude observations. *JASTP*, 149, 87–92, (2016).